Journal of Applied Polymer Science

Synthesis and properties of PMMA-ZrO_2 organic–inorganic hybrid films

Clemente Guadalupe Alvarado-Beltrán,[1] Jorge Luis Almaral-Sánchez,[2] Rafael Ramírez-Bon[1]

[1]Centro de Investigación y de Estudios Avanzados del IPN. Unidad Querétaro, Apdo. Postal 1-798, 76001, Querétaro, Qro., México

[2]Universidad Autónoma de Sinaloa, Fuente de Poseidón y Prol. Angel Flores, S.N., 81200, Los Mochis Sin., México

Correspondence to: R. Ramírez-Bon (E-mail: rrbon@qro.cinvestav.mx)

ABSTRACT: In this work we report the synthesis process and properties of PMMA-ZrO_2 organic–inorganic hybrid films. The hybrid films were deposited by a modified sol-gel process using zirconium propoxide (ZP) as the inorganic (zirconia) source, methyl methacrylate (MMA) as the organic source, and 3-trimetoxy-silyl-propyl-methacrylate (TMSPM) as the coupling agent between organic and inorganic phases. The films were deposited by dip coating on glass slide substrates from a hybrid precursor solution containing the three precursors with molar ratio 1 : 0.25 : 0.25 for ZP, TMSPM, and MMA, respectively. After deposition, the hybrid thin films were heat-treated at 100°C for 24 h. The macroscopic characteristics of the hybrid films such as high homogeneity and high optical transparence evidenced the formation of a cross-linked, interpenetrated organic–inorganic network. The deposited PMMA-ZrO_2 hybrid films were homogeneous, highly transparent and very well adhered to substrates. Fourier Transform Infra-Red measurements of the hybrid films display absorption bands of chemical groups associated with both PMMA and ZrO_2 phases. The amounts of organic and inorganic phases in the hybrid films were determined from thermogravimetric measurements. The surface morphology and homogeneity of the hybrid films at microscopic level were analyzed by scanning electron microscopy and atomic force microscopy images. From the analysis of optical transmission and reflection spectra, the optical constants (refraction index and extinction coefficient) of the hybrid films were determined, employing a physical model to simulate the hybrid optical layers. The refraction index of the hybrid films at 532 nm was 1.56. © 2015 Wiley Periodicals, Inc. J. Appl. Polym. Sci. **2015**, *132*, 42738.

KEYWORDS: amorphous; coatings; crosslinking; optical properties; synthesis and processing

Received 20 December 2014; accepted 25 May 2015

DOI: 10.1002/app.42738

INTRODUCTION

Organic–inorganic hybrids materials are a new class of materials that have been exploited to enhance specific properties of the individual components of the hybrid material. For example, the poor mechanical properties of a soft polymer (organic phase) can be improved by appropriately mixing it with a harder metal oxide (inorganic phase).[1–3] The properties of the resultant hybrid material depend mainly on the amount of both phases and the kind of chemical bonding between them .[4–6] In hybrid materials of class I, the components exchange rather weak bonds such as van der Waals, hydrogen bonds or ionic interactions, such as for example, inorganic semiconductor nanoparticles embedded in an organic matrix .[7,8] On the other hand, in hybrid materials of class II the components are bonded through stronger covalent or ionic-covalent chemical bonds, forming a cross-linked interpenetrated hybrid network .[9–12] Hybrid materials represent excellent alternative to attain unique properties which otherwise cannot be found in the single isolated components.[13] That is why hybrid materials have been the focus of intense research in the last few years. Sol-gel process is the most appropriated synthesis method for the deposition of hybrid thin films because it allows the proper linking between the organic and inorganic phases at the molecular level in a hybrid network.[14,15] Additional advantages of the sol-gel method include low temperature processing and high control in the final organic to inorganic phase composition.[11,12] The low temperature is crucial in hybrid materials processing because the low thermal resistance of the organic phases, which typically are polymers, cannot be heated at high temperature.[5,14]

The PMMA-Oxide hybrid systems have been widely reported, mostly focused on SiO_2-PMMA hybrid systems.[5,8,10,13] In class I materials of this hybrid system, the inorganic phase has been embedded in PMMA matrix in the form of nanowhiskers,[16] nanoparticles,[17] nanocrystals,[7] nanotubes,[2] etc. One of the main disadvantages of this type of hybrid materials is the difficulty to disperse the isolated inorganic particles homogeneously in the polymer matrix. The agglomeration produced by the high reactivity of the nanoparticles produces light diffraction or

scattering reducing the optical quality of the materials.[7,8] On the other hand, the incorporation of inorganic network and organic polymerization *in situ* promote the formation of class II hybrid materials avoiding the precipitation of separated phases.[5,9] This results in homogenous hybrid materials at microscopic level with high optical transparency at macroscopic level. To achieve compatibility and enhance the interface between organic and inorganic phases (polymer hydrophobic and metal oxide hydrophilic are immiscible) coupling agents are commonly employed in the synthesis of hybrid materials.[14] In recent papers we have reported the use of TMSPM (3-trimetoxy-silyl-propyl- methacrylate) as an excellent coupling agent for the PMMA-SiO_2 hybrid system.[5,11,14] The incorporation of TMSPM in the hybrid sol-gel precursor solution allows the deposition of PMMA-SiO_2 hybrid films with high optical transparency, very low surface roughness, and low friction coefficient.[11,14,16] Furthermore, the optical, mechanical, and dielectrics characteristics of these hybrid films can be adjusted by controlling the molar ratio of TMSPM in the sol-gel precursor solution.[5,11,16]

Metal oxides such as SiO_2, TiO_2, ZnO, Al_2O_3, and ZrO_2[10,11,16–18] have been successfully employed to increase the refractive index in Polymer-Metal oxide hybrid coatings. For combination in hybrid systems with organic components, ZrO_2 has the advantages of chemical inertness, excellent thermal stability, [17] high refractive index (between 2.15 and 2.18 in bulk), optical transparency in the visible region, high hardness, and scratch and wear resistance.[1,3,16] Several hybrid systems with ZrO_2 as the inorganic phase have been reported in literature, most of them consisting in ZrO_2 nanoparticles embedded in PMMA matrix.[3,7,8,10,17] ZrO_2-PMMA hybrid films have high refractive index, high mechanical properties, and better thermal stability than other hybrid films.[15] The corrosion protection using ZrO_2-PMMA hybrid coating was better than pure inorganic ZrO_2 coatings.[18,19] ZrO_2-PMMA hybrid films reported in Refs. 1,16 present wear behavior and scratch resistance better than those of TiO_2 or SiO_2-based hybrid films. The dielectric properties of PMMA-ZrO_2 hybrid composites have been reported in Refs. 18,20,21, where this hybrid systems is proposed for applications in electronic devices. The main characteristics of the TiO_2/ZrO_2/PMMA hybrid system as reported in Ref. 4 are high refractive index and enhanced thermal stability.

In this article we report the sol-gel process to deposit highly transparent PMMA-ZrO_2 hybrid films. The deposition process is based in our previous works about the deposition of PMMA-SiO_2 hybrid films, where the hybrid materials results from the in situ polymerization of the organic phase during the hydrolysis and condensation of the inorganic one.[5,9,11,14,16] To improve the compatibility between PMMA and ZrO_2, TMSPM was used as coupling agent in addition to organic and inorganic precursors. We also report the properties of the deposited hybrid films characterized by several experimental microscopic and spectroscopic techniques. The results show that the PMMA-ZrO_2 hybrid films are highly homogeneous with high optical quality and transparence in the visible region. Such macroscopic characteristics of the hybrid layers evidence the formation of a cross-linked, interpenetrated organic–inorganic hybrid network.

EXPERIMENTAL

As mentioned above, the sol-gel deposition method to obtain the PMMA-ZrO_2 hybrid films was based on a similar method developed for the deposition of PMMA-SiO_2 films, reported in previous works by our group.[5,9,11,14,16] In the present work, zirconium propoxide (ZP) was used as the inorganic precursor, methyl methacrylate (MMA) as the source of the organic component and 3-trimetoxy-silyl-propyl- methacrylate (TMSPM) as the coupling agent. The polymerization of the MMA monomer was initiated with benzoyl peroxide (BPO). Ethyl alcohol was used as the organic solvent and ethyl alcohol and HNO_3 was used to hydrolyze the inorganic precursor. As solvents for the coupling agent were used HCl and deionized water. The hybrid precursor solution was obtained by mixing the three precursor solutions with molar ratio ZR : TMSPM : MMA (1.0 : 0.25 : 0.25). After stirring for 30 minutes, the resulting homogeneous hybrid solution was used to obtain the hybrid films by dip-coating on conventional glass slide substrates, which were previously cleaned. The wet hybrid films were baked for 24 h in a conventional oven at 100°C and atmospheric pressure. Figure 1 shows the route for the formation of both phases of the hybrid material linked by the coupling agent molecules. The resultant PMMA-ZrO_2 hybrid films were homogeneous, very well adhered to the glass substrates and highly transparent, as observed in the photograph shown in Figure 2. The properties of the hybrid samples were determined from the analysis of Fourier transform infrared (FTIR), thermo gravimetric analysis (TGA), scanning electron microscopy (SEM), atomic force microscopy (AFM), and optical transmission (T) and reflection (R) spectroscopy measurements. The FTIR measurements were performed in the reflectance mode (GA-ATR) mode with a resolution of 4 cm^{-1}, in the wave number range of 400–4000 cm^{-1}, using a Gx Perkin Elmer system. For these measurements, the hybrid films were deposited on Cr/Au (10/100 nm) coated glass substrates. Top view and cross-sectional SEM images of the hybrid films were measured in a Zeiss Supra-40 scanning electron microscope. For this, the hybrid films were previously coated with a thin gold layer. The AFM measurements were done in tapping mode with a Di-Vecco Nanoscope IV instrument. The TGA experiments were performed using a Mettler Toledo Instruments (TGA-851), from room temperature to 1100°C under synthetic air flow (50 mL/min) using a heating rate of 10°C/min. These measurements were done on PMMA-ZrO_2 powder samples obtained by using the same temperature and baking time conditions as those used for the curing of the hybrid films. The T and R spectra of the hybrid films were measured using a thin film metrology system (FilmTek TM 3000, Scientific Computing International) at normal incidence in the UV-visible spectral range (240–840 nm).

RESULTS AND DISCUSSION

In Figure 3 are shown (a) the top view and (b) cross-sectional SEM images of the PMMA-ZrO_2 hybrid film. The surface of the hybrid film at this microscopic level is very uniform, flat, smooth, and free-defect. No separation of phases at the scale of tens of nanometer is observed on the surface. The cross-sectional image shows the transversal homogeneity and

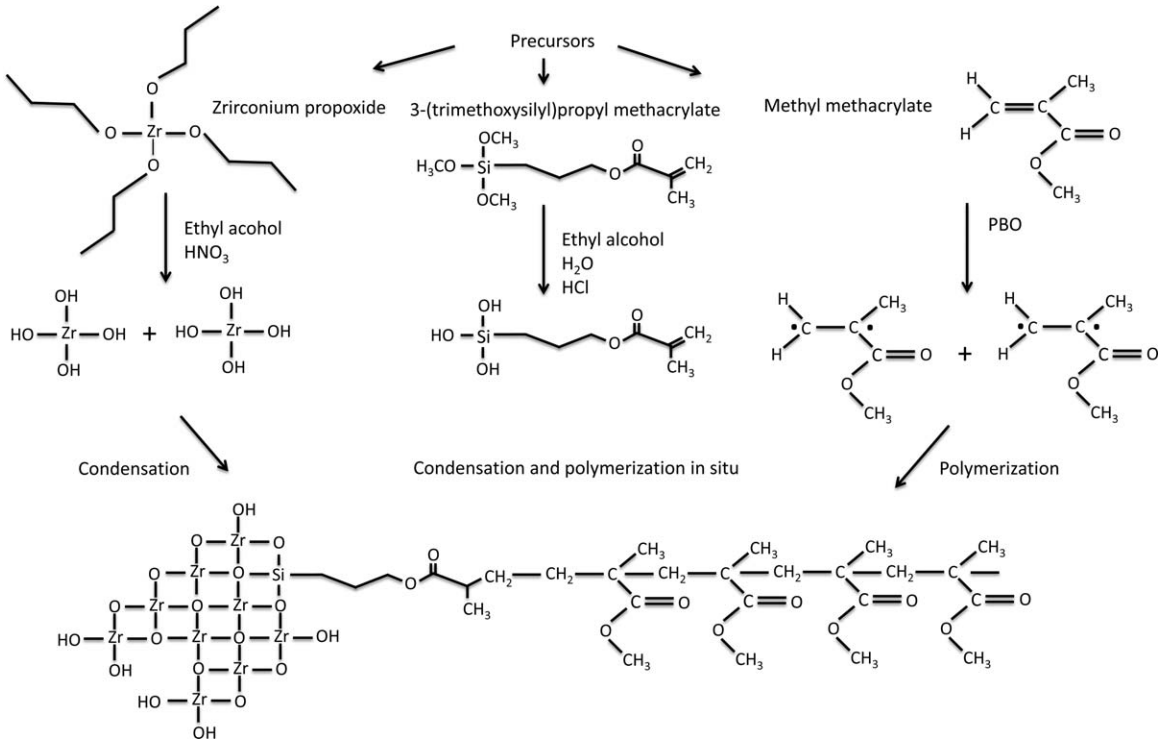

Figure 1. Scheme of the formation of the PMMA-ZrO2 hybrid material.

thickness uniformity of the hybrid film, which is well adhered to the glass substrate. The average thickness of the hybrid film measured from this image is 450 nm. Figure 4 displays the 3-D AFM image of the PMMA-ZrO_2 hybrid film showing its surface morphology. At this magnification it is observable the small grain structure of the hybrid material with size in the order of a few tens of nm. According to the *z*-scale, the distance between highest and lowest heights is of the order of 1 nm. The root mean square (rms) surface roughness of the hybrid film determined from the 1 μm x 1 μm AFM image is 0.36 nm. This is a very low surface roughness value evidencing the flatness and smoothness of the hybrid film surface. The microscopic homogeneity is consistent with the macroscopic homogeneity and optical transparency of the hybrid films, which is attributed to the lack of separated phase precipitation at this nanometric scale. Therefore, the surface and cross-sectional morphology of the hybrid film supports the formation of a hybrid material with homogeneous mixed organic–inorganic network with very small domains at the nanometric scale.[16]

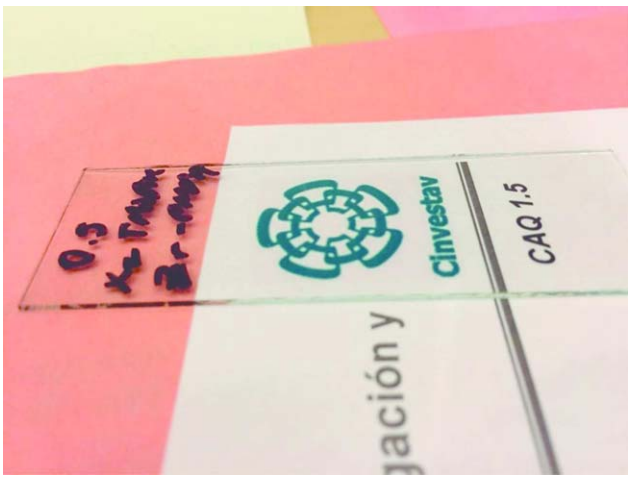

Figure 2. Photograph showing the homogeneity and high optical transparence of the PMMA-ZrO2 hybrid films. [Color figure can be viewed in the online issue, which is available at wileyonlinelibrary.com.]

In Figure 5 it is plotted the TGA curves showing (a) the thermal decomposition of the PMMA-ZrO_2 hybrid films and for comparison that of pure PMMA and (b) the derivative of the weight loss versus temperature curves in (a). The thermal behavior of the hybrid material displays three temperature zones, labeled 1, 2, and 3, respectively. In zone 1, in the 25–230°C temperature range, a nonoxidative degradation is observed, where the weight loss is because of the release of residual solvents from the hybrid network. The small weight loss at this stage is of 7.22%. In the zone 2, between 230°C and 600°C, it is observed a weight drop associated with the oxidative degradation of PMMA. The weight loss is approximately linear in this temperature zone. The thermal behavior of the hybrid film at this temperature zone shows the better thermal stability of the PMMA phase in the hybrid film as compared with isolated PMMA,[22] as shown in the curve for this material. It has been reported that pure PMMA starts the thermal decomposition at about 245°C with complete weight loss at about 400°C[12] or less,[4,7,8] which is in agreement with the thermal behavior of PMMA observed in this graph. In the case of PMMA in the PMMA-ZrO_2 hybrid film, about half its weight is lost at about 400°C and the other half with higher interaction is lost up to about 600°C because in this portion of polymer the chains require higher energy to break. The

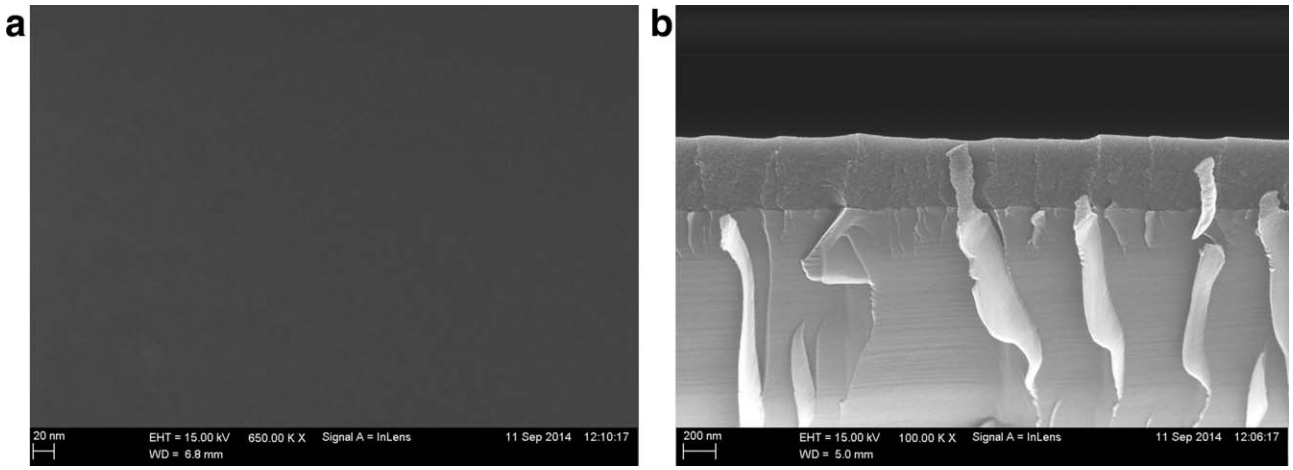

Figure 3. (a) Top view and (b) cross-sectional SEM images of the PMMA-ZrO2 hybrid film.

improved thermal stability of PMMA is because of the interaction of the polymer chains with the inorganic network of zirconia which encloses them and limits their movement.[3,4] Therefore, the behavior under thermodegradation of the hybrid material is another experimental evidence that supports the strong interaction between organic and inorganic phases. The enhancement of the thermal stability of the organic phase in hybrid materials has been assigned to the formation of covalent bonds,[8] which in our case is promoted by the TMSPM coupling agent. In zone 3, at temperatures higher than 600°C, the weight of the hybrid material stabilizes at about 48.84%. This is the remaining of the hybrid sample which corresponds to the inorganic part, because the solvents and organic phase have been completely removed at this range of temperature. Based on this analysis the weight content (%) of each phase and remaining solvents in the hybrid film was estimated and the results are shown in the graph. In Figure 5(b), the graph for PMMA displays an intense, inverted band, which represents the thermal decomposition of PMMA in the 250–400°C temperature range. For the PMMA-ZrO_2 material, the band is less intense and much broader, from about 200°C to 600°C, evidencing the higher temperature required to decompose the PMMA phase linked to ZrO_2.

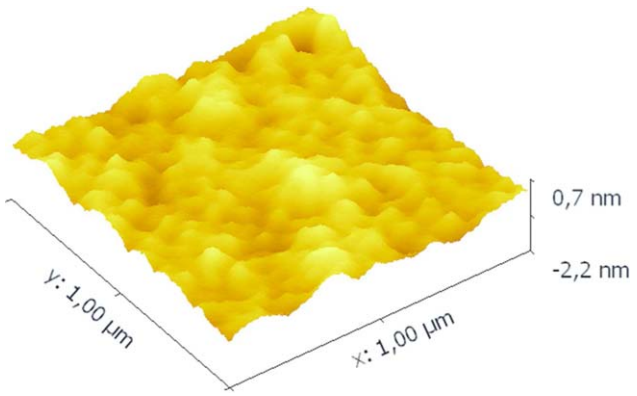

Figure 4. 3-D AFM image of the PMMA-ZrO2 hybrid films. [Color figure can be viewed in the online issue, which is available at wileyonlinelibrary.com.]

Figure 6 shows the FTIR spectrum of the PMMA-ZrO_2 hybrid film in the 400–4000 cm^{-1} wavenumber range. In this graph, the most intense and evident absorption bands are labeled with their corresponding vibration modes, which identify the chemical groups in the hybrid material. The wide and strong band centered at about 3460 cm^{-1} is attributed to O-H stretching

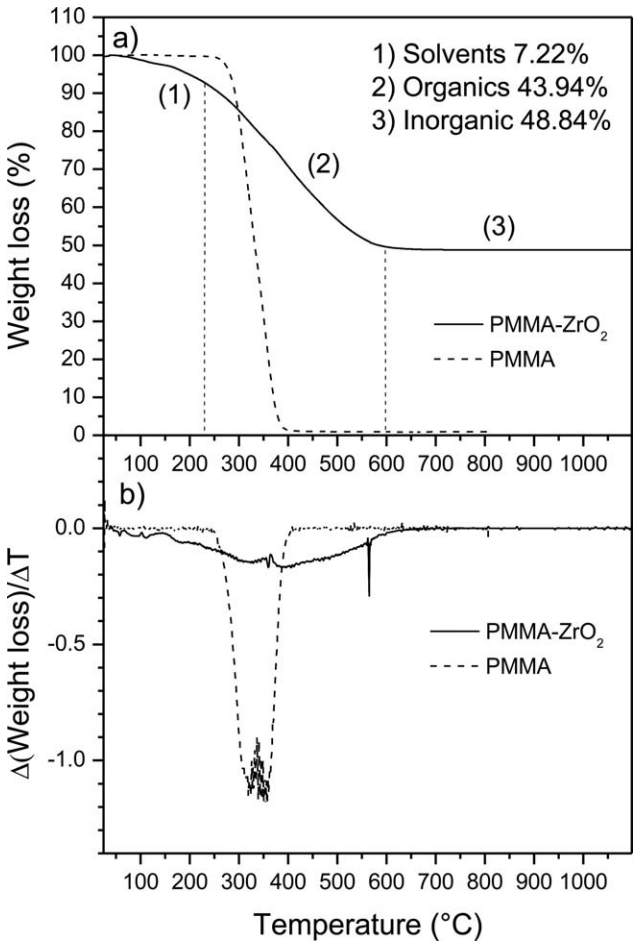

Figure 5. (a) Thermal decomposition graph of the PMMA-ZrO2 and PMMA materials. (b) Derivative of the graphs in (a).

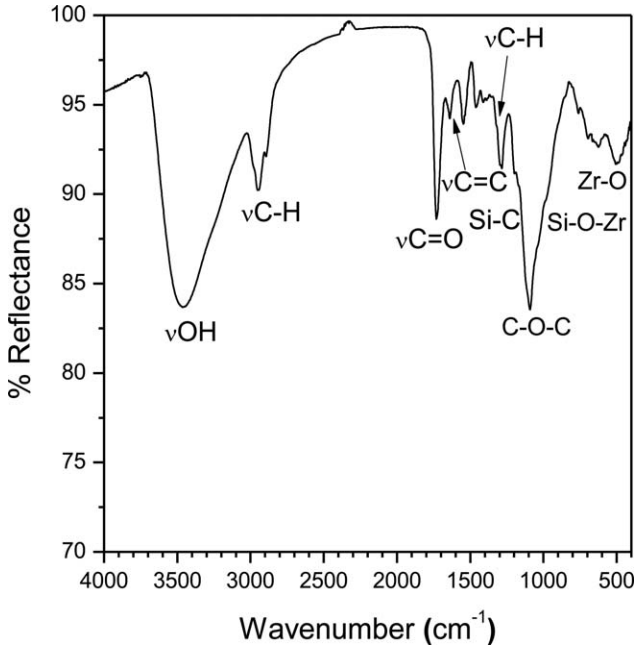

Figure 6. FTIR reflection spectrum of the PMMA-ZrO2 hybrid film.

modes,[9,11,14] which are mainly because of Zr-OH groups resulting from the incomplete condensation of the inorganic component in the sol-gel process.[4,8,17] From TGA measurements it was identified remaining solvents with OH groups, which also contribute to this absorption band. In addition, hydroxyl groups can also adsorb to the surface and have been observed in the FTIR spectra of crystalline ZrO_2 obtained by sol-gel process.[17] The groups associated to the PMMA organic phase are identified with the absorption bands at 2945, 1730, and 1640 cm^{-1} produced by the stretching vibration modes of C-H, C=0, and C=C groups, respectively.[8,17] The C=C groups, contained in the coupling agent and monomer molecules, are the bonding point for the polymerization by free radicals.[4,7] Therefore, the presence of this band in the spectrum is the evidence of some incomplete polymerization of the monomer.[5] The bands at lower wavenumber are associated mainly to the inorganic component. The broad absorption band between 950 and 12,30 cm^{-1} is caused by the overlapping of several vibration modes; at 1075 cm^{-1} there is a band assigned to Si-C bonds from the coupling agent molecules,[4,5,11] at 1060–1100 cm^{-1} there is another band because of C-O-C stretching vibration modes of the acrylic group,[4,7,8] at 1126 cm^{-1} there is a band assigned to Zr-O-C evidencing some incomplete hydrolysis of ZP and at 930 cm^{-1} there has been reported absorption because of vibration modes of Si-O-Zr groups[23] because of the interaction between the inorganic phase and the organic one bonded through the coupling agent molecule.[4,7] The formation of ZrO_2 material in the hybrid matrix is evidenced by the signals observed at ~500 cm^{-1} and ~620, which are related with the vibration modes of the Zr-O groups.[2,4,7,8,17] Based on the groups identified by the FTIR analysis it is possible to get some insight about the reaction mechanism which takes place during the formation of the organic–inorganic hybrid network. At the beginning of the process, the hydrolysis of TMSPM molecules originates Si-OH groups, which can bind with the Zr-OH groups of the ZP inorganic precursor to form Si-O-Zr groups.[4] The high reactivity of the inorganic precursor (ZP) in the aqueous medium promotes a fast hydrolysis favoring the condensation process for the growth of the inorganic amorphous network constituted by Zr-O-Zr groups.[8] On the other hand, the hydrophobicity of the organic molecules produces the isolated growth of polymeric chains. The free radicals method allows the polymerization by breaking the C=C groups of the monomer molecules and binding to one extreme of the coupling agent molecules with some selectivity because of the hydrophobicity.

The optical transmission (T) and reflection (R) spectra of the PMMA-ZrO_2 films are shown as solid lines in Figure 7. For comparison it is also included in this graph the corresponding T and R spectra of the glass substrate. It is observed that hybrid films is highly transparent in the visible region with average T value of ~90%, of the same order as that observed in the T substrate spectrum. The sharp cut-off of the transmission spectrum at about 340 nm is produced by the optical absorption of the glass substrate. The R spectrum displays oscillations above the R substrate spectrum with minimum values at points coinciding with the R curve of the substrate, approximately. Furthermore, it is also observed in these optical spectra that $R+T$ values in the transparent region are very close to 100%, showing that the PMMA-ZrO_2 film is nonabsorbing and the light scattering is negligible. In some reports of the optical properties of PMMA-ZrO_2 films it is difficult to assess its quality because the reflectance spectra of the hybrid films are not included.[3,4,7,8,13,15,19] The features in the optical spectra of our PMMA-ZrO_2 hybrid film are indications of its high optical quality and that it has higher refraction index than the glass substrate. The high optical transparency of the hybrid films confirms also the formation of a homogeneous composite material with cross-linked organic

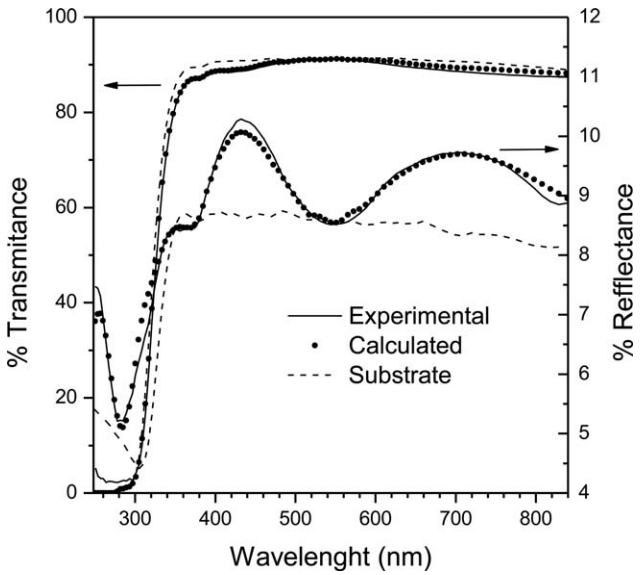

Figure 7. Optical transmittance (T) and reflectance (R) spectra of the PMMA-ZrO2 hybrid film. The solid lines correspond to the measured R and T spectra and the dotted lines are the best fitting to the proposed theoretical model.

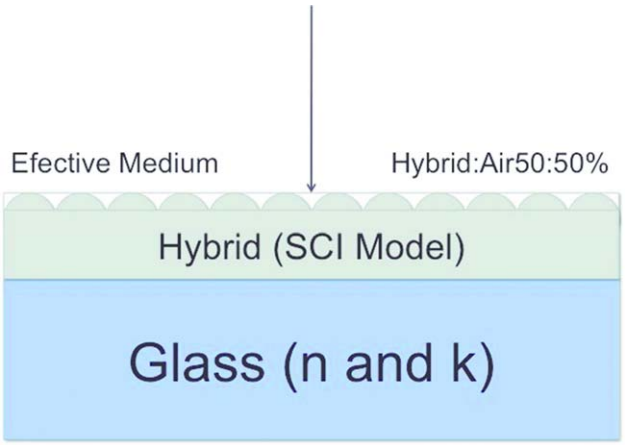

Figure 8. Scheme of the layers model to represent the PMMA-ZrO2 hybrid film deposited on glass substrate. [Color figure can be viewed in the online issue, which is available at wileyonlinelibrary.com.]

and inorganic phases, in which the domains have nanometric dimensions much smaller than the wavelength of light in the visible region, in agreement with the observed microscopic morphology (Figures 3 and 4). Therefore, the hybrid films do not lost light in the visible region, unlike some other hybrid films of the same system which disperse or scatter the light because of nanoparticles agglomeration.[3,7,8,10,13,15,17,19,21]

The dispersion relation to represent the optical constants of the hybrid film is a generalized version of the Lorenz Oscillator Model and the roughness layer was modeled by an effective medium approximation (50% hybrid film and 50% air voids), as described in Ref. 4 and the scheme of the theoretical model is shown in Figure 8. The SCI model used by the FilmWizard software is based in the Lorentz harmonic oscillator expression,[24] which can be written as

$$\varepsilon(E)=\varepsilon_{\infty}\left(1+\sum_{j=1}^{j}\frac{A_j^2}{E_j^2-E^2-iE\Gamma_j}\right)$$

where ε_{∞} is the high-energy dielectric constant, A_j, E_j, and Γ_j are the amplitude, central energy, and broadening parameter of the *j-th* oscillator, respectively. The optical constants of the intermediate and external layers, composed by a mixture of PMMA-ZrO_2 and voids, were modeled by an *effective media* approximation. In particular, it was used Bruggeman model, which is very appropriate for heterogeneous thin films.[24] According to this model, the effective dielectric function, ε, of the layer, obeys the following equation:

$$f_{\text{film}}\frac{\varepsilon_{\text{film}}-\varepsilon}{\varepsilon_{\text{film}}+2\varepsilon}+f_{\text{air}}\frac{\varepsilon_{\text{air}}-\varepsilon}{\varepsilon_{\text{air}}+2\varepsilon}=0$$

where ε_{film} and ε_{air} are the dielectric functions of PMMA-ZrO_2 film and air, respectively, and f_{film} and f_{air} are the volume fraction of PMMA-ZrO_2 and voids (air) in the mixture layer. The best fits of this model to the T and R experimental spectra are plotted as dotted lines in Figure 7, where it is observed very good agreement with the experimental data over the full wavelength range. The film thickness determined from this fit is 410 nm, which agrees with the thickness measured from the cross-sectional SEM image shown in Figure 3(b). Figure 9 displays the optical constant, n and k, obtained also from this fit, as a function of the wavelength. A slight increase of refraction index is observed when wavelength decreases, which is typical behavior of transparent materials in the visible region. At about 350 nm, an abrupt increase of n is observed which is related with the optical transitions at the fundamental absorption edge of PMMA. The refractive index of the PMMA-ZrO_2 hybrid film at 532 nm is $n = 1.57$, much higher than that of the organic phase, $n = 1.49$, and those of other hybrid films reported.[4,7] On the other hand, this value of refraction index is lower than that reported for ZrO_x amorphous films deposited by sol-gel and annealed at 100°C, in Ref. 10 it is reported n=1.60–1.66 for hybrid SPC-ZrO_2 films where the wt % of ZrO_2 nanoparticles is 10–50%, however in these hybrid films it is observed light dispersion because of nanoparticles agglomeration. Consistent with the transparency of the hybrid films, the extinction coefficient is zero in the visible region and the increase at 300 nm is produced by the absorption of light of the organic phase, that is, it corresponds to the absorption edge of PMMA, which energy band gap has been reported to be 4.6 eV.[25] The reported energy band gap of ZrO_2 is in the range 6–6.2 eV. The optical band gap of PMMA phase was determined by calculating the absorption coefficient spectrum, α (λ), of the hybrid films by using the relation $\alpha(\lambda) = 4\pi k / \lambda$ and plotting $(h\nu\alpha)^2$ vs. E, where h is the Planck constant and ν and E are the frequency and photon energy, respectively. This plot is shown in Figure 10. From the Tauc model for amorphous materials the linear behavior in this plot is fitted to a straight line to determine the optical band gap of the material with allowed direct transitions,[26] which in this case is 4.46 eV, very close to the value reported for PMMA.

CONCLUSIONS

In this work we reported the sol-gel method to deposit homogeneous and highly transparent PMMA–ZrO_2 hybrid films on glass substrates. The strong interaction between organic and inorganic

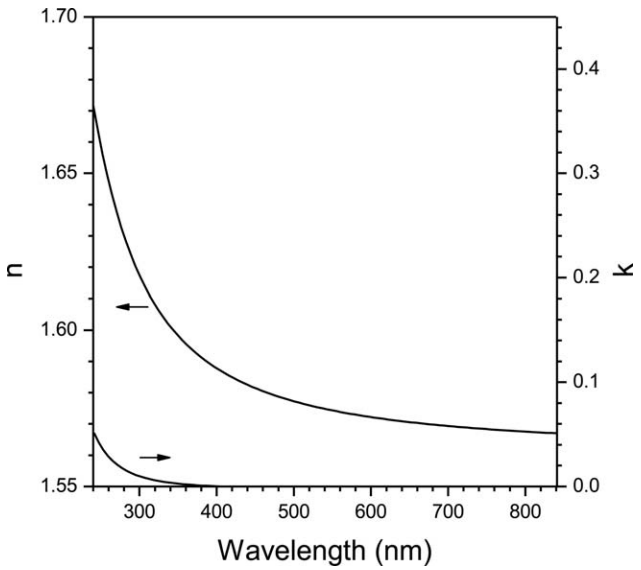

Figure 9. Optical constant n and k of the PMMA-ZrO2 hybrid material as a function of wavelength.

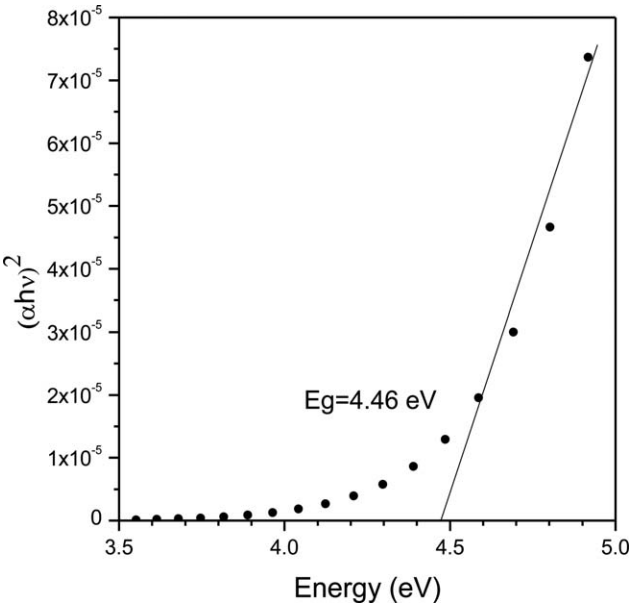

Figure 10. $(\alpha h\nu)^2$ vs E plot of the PMMA-ZrO2 hybrid material in the absorption edge region. The straight line is the best linear fit in this energy region.

phases of the hybrid films is supported by FTIR, TGA, and T and R spectroscopy measurements. SEM and AFM images of the hybrid films show a uniform, smooth, and very flat surface with average roughness lower than 1 nm. The cross-sectional image shows also transversal homogeneity and thickness uniformity. From TGA measurements it was determined the weight content (%) of the organic (48.84%) and inorganic (43.94%) phases and of remnant solvents (7.22%). These measurements also show the improved thermal stability of PMMA phase in the hybrid film as compared to pure PMMA. The thickness, refraction index (at 532 nm), and optical band gap of the hybrid films, as determined from T and R spectroscopy measurements were 440 nm, 1.57 (at 532 nm) and 4.46 eV, respectively. All these results are consistent with hybrid films constituted by a homogeneous organic–inorganic cross-linked network with domain size in the nanometric level, with macroscopic appearance of high optical transparency and uniformity without light losses by scattering.

ACKNOWLEDGMENTS

The technical assistance of R.A. Mauricio-Sánchez, C.A. Ávila-Herrera, J.E. Urbina-Alvarez is gratefully acknowledged.

REFERENCES

1. Akininci, A.; Sen, S.; Sen, U. *Compos. Part B* **2014**, *56*, 42.
2. Yu, W.; Wang, X.; Tang, Q.; Guo, M.; Zhao, J. *J. Mech. Behav. Biomed. Mater.* **2014** *32*, 192.
3. Hu, Y.; Zhou, S.; Wu, L. *Polymer* **2009**, *50*, 3609.
4. Wang, Y.; Zhang, D.; Shi, L.; Li, L.; Zang, J. *Mater. Chem. Phys.* **2008**, *110*, 463.
5. Morales-Acosta, M. D.; Quevedo-Lopez, M. A.; Gnade, B. E.; Ramirez-Bon, R. *J. Sol–Gel. Sci. Technol.* **2011**, *58*, 218.
6. Kunts, S. R.; Piaggio-Cardoso, H. R.; Trindade-Oliveira, C.; da Silva-Filho, C. I.; Victorino-Sarmento, V. H.; Lemos-Menezes, T.; Müller, I. L.; de Fraga-Malfatil, C. *Int. J. Electrochem. Sci.* **2013**, *8*, 11984.
7. Otsuka, T.; Chujo, Y. *Polym. J.* **2010**, *42*, 58.
8. Hu, Y.; Gu, G.; Zhou, S.; Wu, L. *Polymer* **2011**, *52*, 122.
9. Almaral-Sánchez, J. L.; Rubio, E.; Mendoza-Galván, A.; Ramírez-Bon, R. *J. Phys. Chem. Solids* **2005**, *66*, 1660.
10. Imai, Y.; Terahara, A.; Hakuta, Y.; Matsui, K.; Hayashi, H.; Ueno, N. *European Polym. J.* **2009**, *45*, 630.
11. Morales-Acosta, M. D.; Alvarado-Beltrán, C. G.; Quevedo-Lopez, M. A.; Gnade, B. E.; Mendoza-Galván, A.; Ramírez-Bon, R. *J. Non-Cryst. Solids* **2012**, *362*, 124.
12. Khan, S. B.; Rahman, M. M.; Akhtar, K.; Asiri, A. M.; Seo, J.; Han, H.; Alamry, K. *Int. J. Electrochem. Sci.* **2012**, *7*, 4030.
13. Sangermano, M.; Voit, B.; Sordo, F.; Eichhorn, K. J.; Rizza, G. *Polymer* **2008**, *49*, 2018.
14. Martínez-Landeros, V.; Gnade, B.; Quevedo-López, M.; Ramírez-Bon, R. *J. Sol–Gel. Sci. Technol.* **2011**, *59*, 345.
15. Luo, K.; Zhou, S.; Wu, L. *Thin Solids Films* **2009**, *517*, 5974.
16. Alvarado-Rivera, J.; Muñoz-Saldaña, J.; Castro-Beltrán, A.; Quintero-Armenta, J. M.; Almaral-Sánchez, J. L.; Ramírez-Bon, R. *Phys. Status Solidi C* **2007**, *4*, 4254.
17. Nakayama, N.; Hayashi, T. *Compos. Part A* **2007**, *38*, 1996.
18. Devikala, S.; Kamaraj, P.; Athanareeswari, M. *Chem. Sci. Trans.* **2013**, *2*(Suppl 1), S129.
19. Norouzi, M.; Garekani, A. A. *Ceram. Int.* **2014**, *40*, 2857.
20. Messadeeq, S. H.; Pulcinelli, S. H.; Santilli, C. V.; Guastaldi, A. C.; Messaddeq, Y. *J. Non-Cryst. Solids* **1999**, *247*, 164.
21. Sannakki, B.; Anita, *Phys. Proc.* **2013**, *49*, 15.
22. Gross, S.; di Noto, V.; Schubert, U. *J. Non-Cryst. Solids* **2003**, *322*, 154.
23. Shekar, B. C.; Sathish, S.; Sengoden, R. *Phys. Proc.* **2013**, *49*, 145.
24. Valenzuela-Jáuregui, J. J.; Ramírez-Bon, R.; Mendoza-Galván, A.; Sotelo-Lerma, M. *Thin Solid Films* **2003**, *441*, 104.
25. Al-Ammar, K.; Hashin, A.; Husaien, M. *Chem. Mater. Eng.* **2013**, *1*(3), 85.
26. Svorcík, V.; Lyutakov, O.; Huttel, I. *J. Mater. Sci. Mater. Electron.* **2008**, *19*, 363.